Electrochemical Host-Guest Interactions in a Disordered Oligosilyl Coordination Polymer

Rasha I. Anayah[a], Brian G. Diamond[b], Christopher H. Hendon*[b], V. Sara Thoi*[a,c]

Abstract

In this work, we synthesize and study the charge transfer properties of a oligosilyl coordination polymer formed from zirconium clusters. Although the synthesized disordered polymer lacks long range order, spectroscopic and computational evidence suggest that the metal-ligand bond is formed, and the principle crystallographic reflections closely match those simulated from inter-node spacings matching that of the ligand. The porous polymer allows for the incorporation of guest molecules as demonstrated by the intercalation of tetracyanoquinodimethane (TCNQ). Charge transfer is predicted from DFT and experimentally observed by infrared spectroscopy, solid-state ^{29}Si nuclear magnetic spectroscopy, and voltammetry.

Introduction

Silicon-containing materials have been widely explored for semiconducting applications, including as solar absorbers, transistor arrays in computer chips, and for energy storage.[1] The design of silicon materials has been rooted in a top-down approach that involves etching,[2] lithography,[3] and other bulk processing techniques.[4] While these methods are ideal for processability, there is continued interest in developing new silicon-containing molecular materials that afford bottom-up syntheses, providing opportunities for compositional and topological control.[5,6]

Multitopic oligosilane based linkers afford one route to incorporate the silane core into materials via bottom-up synthesis, **Scheme 1**[7-16]. Compared to conventional carbon-based materials, Si atoms can participate in σ-conjugation within the Si–Si chain via primary, geminal, and vicinal interactions.[17,18] The same Si-orbitals are affected by varying chain length and conformation.[19,20] To this end, the electronic properties of oligo- and polysilanes have been studied,[21,22] but there has been limited examples of their incorporation into extended frameworks (**Scheme 1**); we reported the first oligosilane Cu-based MOF in 2020.[10] In addition, prior studies largely concerned the formation of metal-organic frameworks (MOFs) with late transition metals, which have inherent instability at the metal-carboxylate interface. To mitigate this, some effort has been placed in forming framework materials using Group IV metals, Zr from **Scheme 1**, but the linker itself was not an oligosilane.[9]

Building upon the report in Ref 9., we sought to develop a material containing $[Zr_6O_4(OH)_4]^{12+}$ clusters, linked together using an oligosilane from Ref. 10. We hypothesized that these building units should give rise to a stable material where the Zr cluster would not partake in the band edges, thereby allowing us to study any deviation in electronic properties of the ligand as a function of ligation to the cluster. This is important because while there are studies of post-synthetic doping via TCNQ inclusion,[23-25] there are fewer examples of ligand-mediated redox[26], and even fewer examples of how these properties deviate due to the material's assembly.

Like carbon-based aliphatic linkers, oligosilane-containing linkers are inherently flexible. When paired with Zr clusters, it proved difficult to isolate single crystals. As this paper will describe, these materials typically form disordered coordination polymers (dCPs) with crystallographic reflections matching the expectation for a *trans*-connected series of Zr-clusters. While this presents some challenges for topological characterization, most framework materials feature highly localized electronic structure; *i.e.*, the electronic properties of the framework do not primarily depend on the 3D ordering, but rather are dictated by the free motifs themselves. Since our oligosilanes are unlikely to form aggregate, and the *trans* configuration being more stable (due to the increased σ conjugation, see computational details in Supporting Information), we can surmise that materials constructed therefrom should feature electronic properties dictated by the free *trans*-linker itself.

Here, we expand upon the library of materials that feature oligosilane linkers [**lin-Si-2**, $Si_2Me_4(C_6H_4CO_2)_2$] and present **Zr-dCP-Si-2**, an electroactive disorder coordination polymer

whose redox properties are dictated by the linker. Using a combined spectroscopic, electrochemical, and computational approach, we demonstrate that the oligosilyl linkers bind to the Zr clusters and form an extended porous network. The material maintains optical and electron chemical properties akin to the linker itself, which modulates the redox potential of redox active guests. Electronic structure calculations support the hypothesis that the metal clusters do not impact the band edges, bolstering a central design principle of framework chemistry: electronic properties are generally informed by the isolated components of the material.

Scheme 1: Si-containing linkers have been included in frameworks comprised of Zn, Cd, Zr, and Cu. In this work, we combine the linker, $Si_2Me_4(C_6H_4CO_2H)_2$, with the zirconium node to yield a disordered coordination polymer.

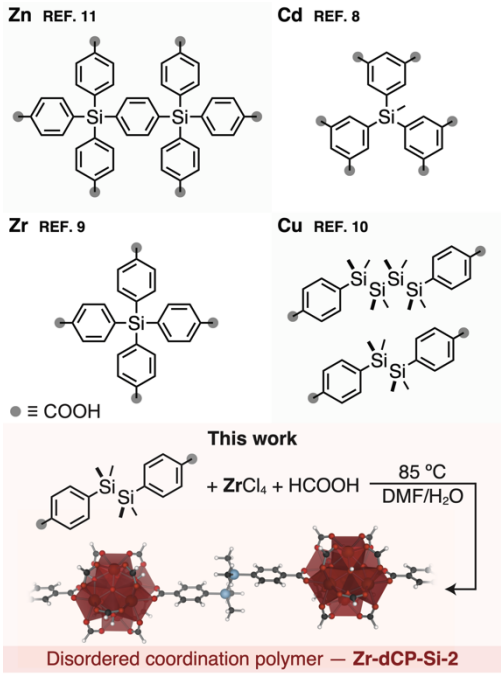

Results and Discussion

To assess the redox chemistry of a framework material comprising the **lin-Si-2** linker, we synthesized an oligosilane dCP containing a redox inert zirconium node. These nodes, commonly found in UiO-66, MOF-808, and NU-1000, act as a skeleton to suspend the oligosilane in a *trans*-conformer as required for sigma conjugation.[27] While some MOFs do crystalize with flexible linkers,[28-32] (*e.g.* UiO-66 derivatives,[28] COK-69[32]) we expected disorder due to the increased size of the linker (affecting the crystallization kinetics)[33] paired with the 12-connected node. We varied the solvent conditions and ratio of linker to modulators in an effort to improve crystallinity,[34] which yielded products ranging from gels to semi-crystalline powder. The most crystalline sample was obtained using 24 equivalents of formic acid per $ZrCl_4$, denoted here as **Zr-dCP-Si-2** (**Scheme 1, Table S1)**, and featured a Type II N_2 adsorption isotherm with a surface area of 197.5 m^2 g^{-1}.

Despite numerous attempts, we were unable to obtain crystals large enough for single crystal X-ray crystallography.

Powder XRD (PXRD) of the as-synthesized product show dominant peaks resolution at 2Θ = 5.2°, 7.4°, and 10.4°. **(Figure 1d).** A more resolved PXRD was obtained of the suspend solid upon sonication, which was attributed to the separation of large amorphous components from the polycrystalline solid. From a 1D computational model system, we were able to simulate some expected reflections associated with repeating structural motifs in the experimental system (structure provided in **Figure S8).** Although there are rare reports of MOFs formed from Zr_8, Zr_9, and Zr_{12} nodes,[35–41] we used the most commonly reported $[Zr_6O_4(OH)_4]^{12+}$ node for our calculations. Using the periodic model, the inter-cluster spacing was manually adjusted to simulate their separation. At internode separations equal to the length of the rigid DFT predicted size of the *trans*-oriented linker, we predict a reflection of 2Θ = 5.0°, aligning with the experimental reflection at 5.2°. We attribute this reflection to internodal separation, with the deviation being due to imperfect *trans* connectivity, a characteristic that is expected with flexible linkers.

To assess the stoichiometry and thermal stability of **Zr-dCP-Si-2**, the dCP was heated to 800 °C at a rate of 5 °C/min and the mass measured via thermogravimetric analysis (TGA, **Figure 1b**). There were three main areas of mass loss corresponding to i) solvent trapped within the pores, ii) modulator bound to the node, and iii) decomposition of the organic the linker, in order of increasing temperature. The mass remaining at 800 °C is attributed to ZrO_2 from the metal nodes and SiO_2, which was confirmed by TGA of the pure linker (**Figure S4**).

Since the monocarboxylate modulators competitively bind to the node and the synthesis requires a high ratio of modulators compared to linker,[42,43] this is an indication that the rate of **lin-Si-2** ligation is relatively slow. To determine its composition, ^{1}H NMR of the base-digested dCP revealed integration signals corresponding to a ratio of 2.29:1 formate:**lin-Si-2** (**Figure 1c**). Elemental analysis through inductively coupled plasma optical emission spectrometry (ICP-OES) showed a Zr:Si molar ratio of 1:2. Assuming the presence of Zr_6 nodes, we deduce the composition of **Zr-dCP-Si-2** to be $[Zr_6O_4(OH)_4]$ $[Si_2Me_4(C_6H_4CO_2)_2]_{6-x}[HCO_2]_{2x,}$ where x is between 3 and 4, highlighting the disordered nature of the coordination polymer.

The oligosilane has several characteristic ATR-IR signals, which can be used to assess the local environment of the linker. The bands at 1400 cm^{-1}, 1250 cm^{-1}, and 1100 cm^{-1} corresponding to COO^-, Si-CH_3, and Si-Ph, respectively (**Figure 1a**).[8] The binding of **lin-Si-2** linker to the zirconium clusters is readily observed using the same technique (**Figure S3**), showing a red shift in vibrational frequency associated with the increased reduced mass of the Zr-cluster compared to the protonated linker. This result was also predicted from our DFT models, which suggested that the linker C=O stretch should red-shift by ~100 cm^{-1} upon ligation to the Zr cluster, qualitatively aligning with experiment (**Figure S8**). From our prior work, we have shown the red shifting of the carbonyl stretch indicates metal ligand bond formation, as the carbonyl is now oscillating near a heavy metal node.[44]

Given the extended **Zr-dCP-Si-2** features both the oligosilane and Zr cluster, we turn our interest to its emergent electronic properties. Taking inspiration from MOFs with host-guest interactions between electron donors and acceptors,[45] we incorporated electron accepting 7,7,8,8-tetracyanoquinodimethane (TCNQ) as a probe to elucidate the reducing behavior of the dCP. TCNQ was sublimed into the dCP by heating to 80 °C under static vacuum, yielding **Zr-dCP-Si-2@TCNQ**. Upon sublimation into the dCP, we observe a color change of the mixture from a pale orange yellow to a green powder.

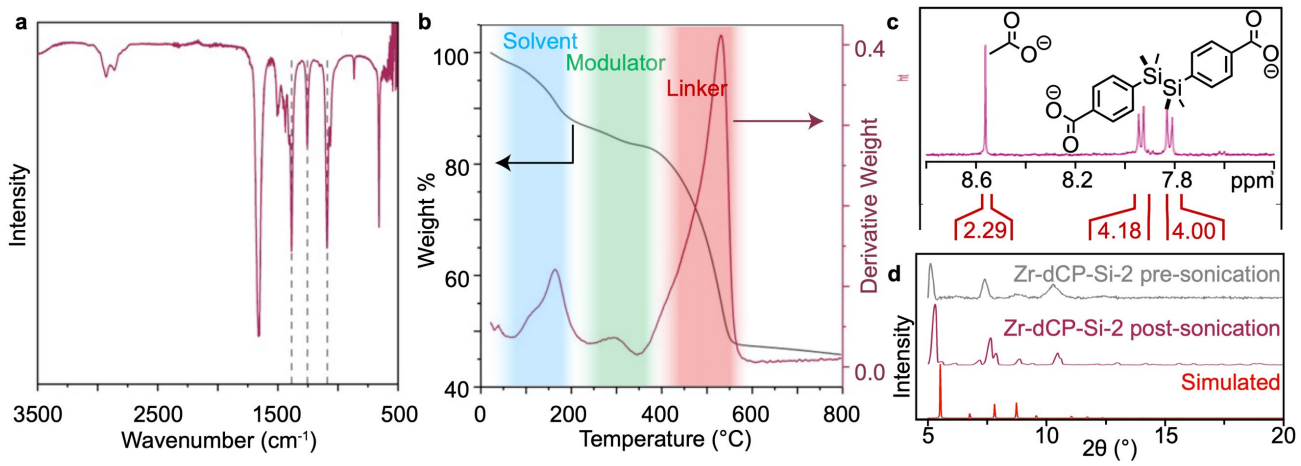

Figure 1. (a) ATR-IR of Zr-dCP-Si-2. (b) Thermogravimetric analysis from 20 °C to 800 °C under argon atmosphere. Distinct peaks in the derivative curve correspond to the loss of solvent, modulator, and organic components of the linker. (c) ^{1}H NMR of digested Zr-Si-2 dCP. dCP was soaked in concentrated NaOH in D_2O overnight. The aromatic protons of the linker are at 7.82 ppm and 7.94 ppm and the formate proton is at 8.56 ppm. Integral values are denoted in red. (d) PXRD of Zr-dCP-Si-2 after sonication compared to DFT-simulated pXRD.

To better understand the nature of these color shifts, we developed a series of DFT models to predict electronic gaps and relative band alignments, **Figure 2**. We computed the energetics of the linker, the formate-passivated Zr_6 cluster, and free TCNQ (**Figure 2**) and their electron energies were aligned to the vacuum level. A molecular fragment of the coordination polymer was computed — a single linker bound to one position on the Zr-cluster — and the resulting electron energies were then aligned. By comparison, the **lin-Si-2** linker comprises the highest energy electron, both in the free linker and dCP cluster, and maps to the general prediction that the properties of the polymer should be dictated by the linker itself. The conduction band of the cluster and, separately, the linker were found to be approximately 2.0 V from vacuum, indicating a predicted degree of orbital in the conduction band. Through alignment with TCNQ, the TCNQ LUMO is predicted to sit mid-gap relative to the dCP conduction band (-5.1 eV), suggesting that charge transfer from the linker to TCNQ is the most favorable electron transfer pathway. These results are in line with the experimental observation that the **lin-Si-2** is oxidized in the presence of TCNQ and also closely match previous experimental reports.[46,47]

We measured the diffuse-reflectance (DR) UV-vis spectra of the samples, and their corresponding Tauc plots for both the solid state (**Figure 3a**) and solution state (**Figure S10**). The resulting band gaps were calculated from the DR-UV-Vis spectra. The bandgap of 4.07 eV for **lin-Si-2** is essentially preserved upon polymer formation; the bandgap of **Zr-dPC-Si-2** is 3.96 eV. TCNQ has a gap of 3.02 eV (in close agreement with the transport gap, ~2.9 eV)[46] The latter shifts ~0.1 eV to 2.95 eV when incorporated with **Zr-dPC-Si-2@TCNQ** (**Table S2**). We note that the DFT under estimation of the TCNQ gap is a well-studied problem related to the treatment of electron exchange, but qualitatively does not change our analysis.

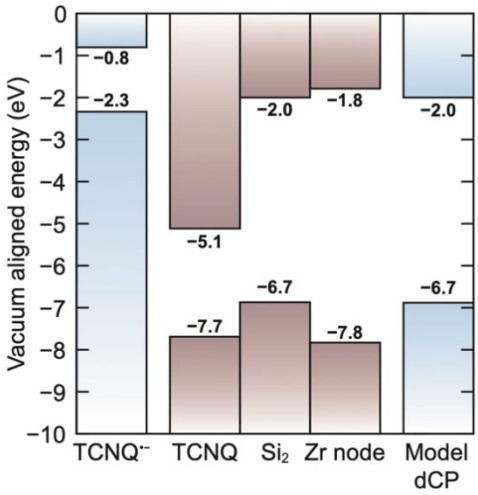

Figure 2. DFT computed electronic structure of the components and model disordered coordination polymer. The material gleans its properties from the linker (Si_2), which is predicted to sit in a Type I semiconductor offset relative to the Zr node. The LUMO of TCNQ sits mid gap relative to the valence band edge and acts as an electron acceptor from the framework. Upon TCNQ being reduced, the highest energy electron sits negative 0.3 eV relative to the framework LUMO, resulting in a metastable TCNQ-framework charge transfer complex.

With these relative alignments in mind, low concentrations of thermally promoted charge transfer from the dCP to TCNQ is expected. The extent of charge transfer interactions was then measured by attenuated total reflectance-infrared spectroscopy (ATR-IR). As the neutral TCNQ is reduced to radical anion (and subsequently a dianion), the C-N bond frequency red-shifts due to the reduced conjugation with the aromatic ring. We observe a change from 2222 cm^{-1} to 2183 cm^{-1} in Zr-**dCP-Si-2@TCNQ**, suggesting a single electron reduction of TCNQ in the framework (**Figure 3b**). This is in close agreement with our DFT predicted C-N stretching frequency shift from 2247 cm^{-1} to 2196 cm^{-1} upon single electron oxidation of molecular TCNQ (See Supporting Information for computational details). Previous literature also reports a similar magnitude of this change in the stretch frequency.[48]

The **lin-Si-2@TCNQ** interaction is also observed by solid-state NMR. The ^{29}Si spectra of the oligosilane and of **Zr-dCP-Si-2** both have a peak centered at -11.2 ppm, indicating that the chemical environment of Si is unchanged when bound within the dCP (**Figure 4**). Once the TCNQ is sublimed into **Zr-dCP-Si-2**, there is a 1.3 ppm upfield shift of the ^{29}Si peak to -12.5 ppm. Predicting chemical shifts in ^{29}Si NMR is non-trivial;[49] thus, we hesitate to remark on the direction of the shift other than the small change in peak position indicates a change in the Si chemical environment in the framework upon TCNQ intercalation.

Finally, because the TCNQ sits mid-gap relative to the dCP, it is not expected to be stoichiometrically oxidized by simple exposure. Instead, the electrochemical properties of the ligand and guest-host framework is comprehensively investigated using cyclic voltammetry (**Figure 5**). A three-electrode system was used with glassy carbon serving as the working electrode, Pt as the counter, and Ag wire with glass frit as the reference electrode with a supporting electrolyte of 0.1 M tetrabutylammonium hexafluorophosphate ($TBAPF_6$) in DMF.

All CVs were first scanned anodically, starting at the open circuit potential. In the CV of **lin-Si-2** (**Figure 5a**), we observe two oxidative peaks at 0.54 V and 1.04 V vs. Fc/Fc^+. We attribute the peak at 1.04 V (marked with an asterisk) to the oxidation of the oligosilane; a peak at the same location is observed in the brominated version of the linker and agrees with previous literature values (**Figure S14**).[20] In the CV of **Zr-dCP-Si-2** that was deposited on a carbon electrode, the

silane oxidative feature (*) is notably retained (**Figure 5b**), although with a minor anodic shift of 40 mV, asserting that the electrochemical behavior of the oligosilane is retained within the dCP. The features at 0.56 V and -2.06 V are attributed to the reduction of carboxylates present in the modulators of the dCP. The small reversible feature at 0 V corresponds to oxygen redox due to a minor leak in the cell.

We sought to understand how the intercalation of TCNQ affects its two-electron redox couple. TCNQ exhibits two reversible redox features at $E_{1/2}$= -0.70 V for the $TCNQ^{2-}/TCNQ^{\bullet-}$ transition and $E_{1/2}$= -0.095 V for the $TCNQ^{\bullet-}$/TCNQ transition (blue dashed lines, **Figure 5c,d**). When **lin-Si-2** and TCNQ are dissolved in solution (equimolar, 10 mM), we observe a shift of 95 mV in the $E_{1/2}$ of the $TCNQ^{2-}/TCNQ^{\bullet-}$ and 105 mV in the $E_{1/2}$ of the $TCNQ^{\bullet-}$/TCNQ (green dashed lines, **Figure 5c**). The minor peak in the reduction at -0.7 V is likely residual TCNQ that has not complexed with **lin-Si-2**. In the intercalated **Zr-dCP-Si-2@TCNQ** (**Figure 5d**), we observe identical shifts in the two TCNQ transitions. These negative shifts in $E_{1/2}$ suggest there is increased electron density on the TCNQ upon interaction with the oligosilane linker, thereby making the complexed TCNQ more readily oxidized. The similar magnitude of changes in $E_{1/2}$ between **lin-Si-2** and **Zr-dCP-Si-2** with TCNQ, further suggesting that the Zr nodes serve primarily as a structural support in the dCP and minimally affect electronic structure of the oligosilane linker.

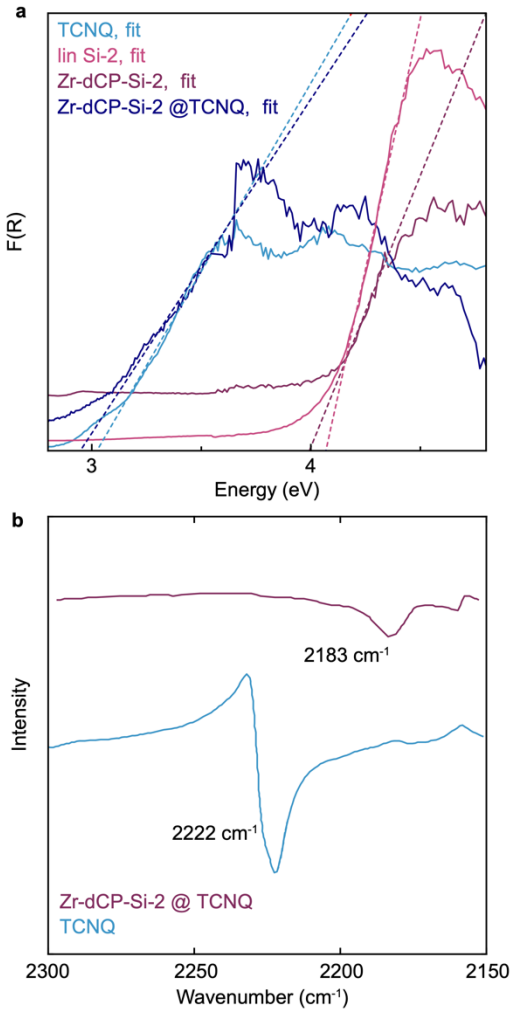

Figure 3. **(a)** Tauc plot of TCNQ (light blue), lin-Si-2 (pink), Zr-dCP-Si-2(purple), and Zr-dCP-Si-2@TCNQ(dark blue) with corresponding fits extrapolated to the x-axis. The x-intercept corresponds to the band gap. **(b)** ATR-IR of TCNQ nitrile stretch before (light blue) and after (dark

blue) intercalation within the dCP. The shift in the nitrile stretch frequency from 2222 cm^{-1} to 2183 cm^{-1} corresponds to a single electron reduction of TCNQ.

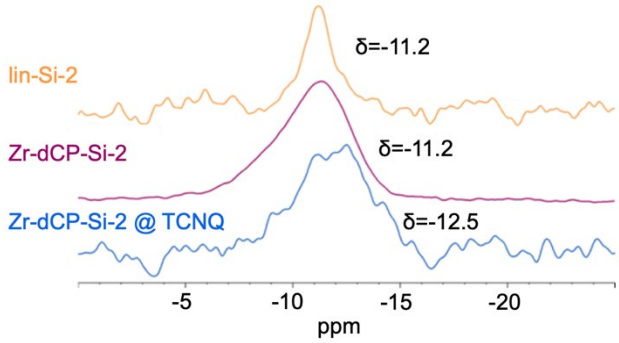

Figure 4. Solid-State ^{29}Si MAS NMR. lin-Si-2, Zr-dCP-Si-2, and Zr-dCP-Si-2 intercalated with TCNQ. Samples were referenced to tetrakis(trimethylsilyl) silane. The Si peak is preserved from linker to dCP and shifts -1.3 ppm upon intercalation with TCNQ.

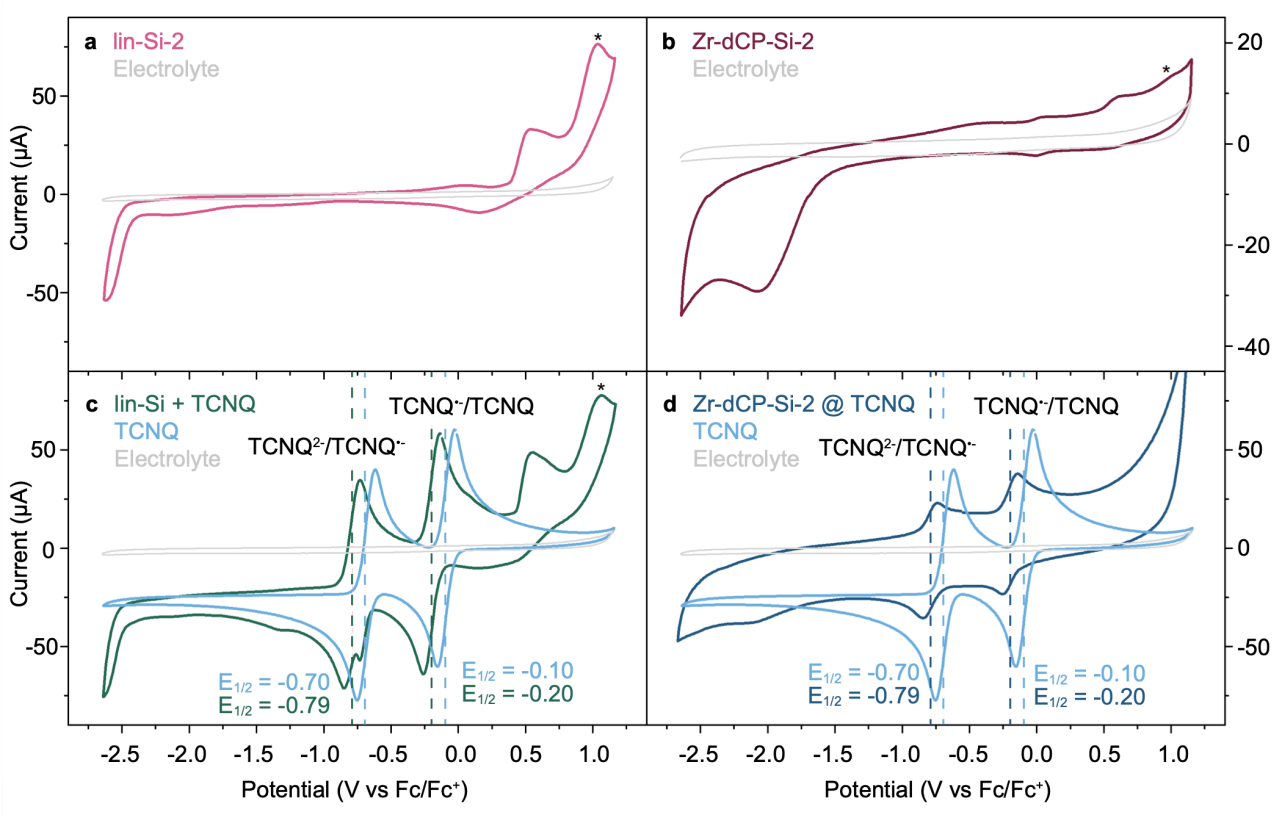

Figure 5. Cyclic voltammograms of **(a)** lin-Si-2, **(b)** Zr-dCP-Si-2, and **(c)** TCNQ with and without lin-Si-2 and **(d)** TCNQ and Zr-dCP-Si-2@TCNQ. dCP samples were drop cast onto the glassy carbon electrode as a slurry of 2 mg/mL of 1:2 graphene oxide: dCP in isopropanol. All CVs were taken in 0.1 M $TBAPF_6$ in DMF at a scan rate of 100 mVs^{-1} and referenced to an external Fc/Fc^+ reference. The gray dashed line indicates the $E_{1/2}$ position of the TCNQ features, and the red dashed line indicates the $E_{1/2}$ position after interaction with the respective species. The asterisk (*) indicates the oxidation of the silyl group in the linker as reported previously.[20]

Conclusion

Together, we have presented a comprehensive assessment of the composition and physical properties of a disordered coordination polymer comprising Zr clusters supported by oligosilane ditopic linkers. Our bottom-up approach resulted in the retention of the oligosilane electronic properties upon material formation. Coupling the structural and DFT analysis, we then demonstrated that the metal cluster does not affect the properties of the linker, as evidenced by the electrochemical behaviour of **Zr-dCP-Si-2@TCNQ** composite. Together, the study demonstrates that oligosilane linkers are expected to retain their properties upon incorporation into a framework and should motivate their implementation in future bottom-up approaches.

Author Contributions

R. I. A. designed and conducted the experimental procedures and analyzed the data. B. G. D. and C. H. H. conducted the theoretical calculations. V. S. T. designed the experimental procedures and analyzed the data. The manuscript was written through contributions of all authors.

Conflicts of interest

There are no conflicts to declare.

Acknowledgements

We thank the National Science Foundation for the CAREER Award (DMR-1945114) and CAREER Award (CHE-2237345). We also are thankful for a Major Research Instrumentation grant (MRI-2018176), which enabled the acquisition of a solid-state 500 MHz Nuclear Magnetic Resonance spectrometer. This work used Expanse at SDSC through allocation CHE230104 from the Advanced Cyberinfrastructure Coordination Ecosystem: Services & Support (ACCESS) program, which is supported by National Science Foundation grants #2138259, #2138286, #2138307, #2137603, and #2138296. We thank Prof. Rebekka Klausen (Johns Hopkins University) for insightful discussions and initiating our interest in this area. We thank Dr. David Burns and Dr. Kyle Barcus for synthesis and crystallization advice, Dr. Carter Gerke for his assistance with electrochemical experiments and SEM, Mr. Sreyas Chintapalli for his help with UV-Vis spectroscopy, and Dr. Jonathan Catazaro (Johns Hopkins University) for his assistance in solid-state NMR experiments. We also thank Mr. Ian Dillingham and Dr. Carter Gerke for proofreading this manuscript. R. I. A. dedicates her contribution to this paper to her grandmother who passed away as this project was being completed. V. S. T and C. H. H. are grateful for the support from the Camille and Henry Dreyfus Foundation.

Notes and references

1 An, Y.; Tian, Y.; Wei, C.; Zhang, Y.; Xiong, S.; Feng, J.; Qian, Y. Recent Advances and Perspectives of 2D Silicon: Synthesis and Application for Energy Storage and Conversion. Energy Storage Mater. 2020, 32, 115–150. https://doi.org/10.1016/j.ensm.2020.07.006.

2 Sreejith, K. P.; Sharma, A. K.; Basu, P. K.; Kottantharayil, A. Etching Methods for Texturing Industrial Multi-Crystalline Silicon Wafers: A Comprehensive Review. Sol. Energy Mater. Sol. Cells 2022, 238, 111531. https://doi.org/10.1016/j.solmat.2021.111531.

3 Chason, E.; Picraux, S. T.; Poate, J. M.; Borland, J. O.; Current, M. I.; Diaz de la Rubia, T.; Eaglesham, D. J.; Holland, O. W.; Law, M. E.; Magee, C. W.; Mayer, J. W.; Melngailis, J.; Tasch, A. F. Ion Beams in Silicon Processing and Characterization. J. Appl. Phys. 1997, 81 (10), 6513–6561. https://doi.org/10.1063/1.365193.

4 Tintelott, M.; Pachauri, V.; Ingebrandt, S.; Vu, X. T. Process Variability in Top-Down Fabrication of Silicon Nanowire-Based Biosensor Arrays. Sensors 2021, 21 (15), 5153. https://doi.org/10.3390/s21155153.

5 Miller, R. D.; Michl, J. Polysilane High Polymers. Chem. Rev. 1989, 89 (6), 1359–1410. https://doi.org/10.1021/cr00096a006.

6 Abe, A.; Jeu, W. H. D.; Kobayashi, S.; Leibler, L.; Long, T. E.; Manners, I.; Terentjev, E. M.; Vicent, M.; Voit, B.; Wegner, G.; Wiesner, U. Advances in Polymer Science - Silicon Polymers.

7 Davies, R. P.; Less, R. J.; Lickiss, P. D.; Robertson, K.; White, A. J. P. Tetravalent Silicon Connectors Me n Si(p -C 6 H 4 CO 2 H) 4− n (n = 0, 1, 2) for the Construction of Metal−Organic Frameworks. Inorg. Chem. 2008, 47 (21), 9958–9964. https://doi.org/10.1021/ic801174d.
8 Tian, H.-R.; Gao, C.-Y.; Yang, Y.; Ai, J.; Liu, C.; Xu, Z.-G.; Sun, Z.-M. A Microporous Cd-MOF Based on a Hexavalent Silicon-Centred Connector and Luminescence Sensing of Small Molecules. New J. Chem. 2017, 41 (3), 1137–1141. https://doi.org/10.1039/C6NJ03470E.
9 Wang, S.; Wang, J.; Cheng, W.; Yang, X.; Zhang, Z.; Xu, Y.; Liu, H.; Wu, Y.; Fang, M. A Zr Metal–Organic Framework Based on Tetrakis(4-Carboxyphenyl) Silane and Factors Affecting the Hydrothermal Stability of Zr-MOFs. Dalton Trans. 2015, 44 (17), 8049–8061. https://doi.org/10.1039/C5DT00421G.
10 Burns, A. D. A.; Press, E. M.; Siegler, M. A.; Klausen, S.; Thoi, V. S. 2D Oligosilyl Metal-Organic Frameworks as Multi-State Switchable Materials. *Angew. Chem. Int. Ed.* 2020, 59 (2) 763–768. https://doi.org/10.1002/anie.201912911.
11 Davies, R. P.; Lickiss, P. D.; Robertson, K.; White, A. J. P. An Organosilicon Hexacarboxylic Acid and Its Use in the Construction of a Novel Metal Organic Framework Isoreticular to MOF-5. CrystEngComm 2012, 14 (3), 758–760. https://doi.org/10.1039/C1CE06091K.
12 Hui, Y.-F.; Kang, C.-L.; Tian, T.; Dang, S.; Ai, J.; Liu, C.; Tian, H.-R.; Sun, Z.-M.; Gao, C.-Y. Metal–Organic Frameworks Constructed from a Tetrahedral Silicon-Based Linker for Selective Adsorption of Methylene Blue. CrystEngComm 2017, 19 (11), 1564–1570. https://doi.org/10.1039/C6CE02639G.
13 Timokhin, I.; Baguña Torres, J.; White, A. J. P.; Lickiss, P. D.; Pettinari, C.; Davies, R. P. Organosilicon Linkers in Metal Organic Frameworks: The Tetrahedral Tetrakis(4-Tetrazolylphenyl)Silane Ligand. Dalton Trans. 2013, 42 (38), 13806–13808. https://doi.org/10.1039/c3dt51863a.
14 Lambert, J. B.; Liu, Z.; Liu, C. Metal - Organic Frameworks from Silicon- and Germanium-Centered Tetrahedral Ligands. Organometallics 2008, 27 (7), 1464–1469. https://doi.org/10.1021/om701262m.
15 Gupta, V.; Khullar, S.; Kumar, S.; Mandal, S. K. Construction of a Robust Pillared-Layer Framework Based on the Rare Paddlewheel Subunit [Mn II 2 (μ-O2CR)4L2]: Synthesis, Crystal Structure and Magnetic Properties. Dalton Trans. 2015, 44 (38), 16778–16784. https://doi.org/10.1039/c5dt02354h.
16 Davies, R. P.; Less, R.; Lickiss, P. D.; Robertson, K.; White, A. J. P. Structural Diversity in Metal-Organic Frameworks Built from Rigid Tetrahedral [Si(p- C6H4CO2)4] 4- Struts. Cryst. Growth Des. 2010, 10 (10), 4571–4581. https://doi.org/10.1021/cg1008768.
17 Dewar, M. J. S. Chemical Implications of .Sigma. Conjugation. J. Am. Chem. Soc. 1984, 106 (3), 669–682. https://doi.org/10.1021/ja00315a036.
18 Klausen, R. S.; Widawsky, J. R.; Steigerwald, M. L.; Venkataraman, L.; Nuckolls, C. Conductive Molecular Silicon. J. Am. Chem. Soc. 2012, 134 (10), 4541–4544. https://doi.org/10.1021/ja211677q.
19 Sasaki, M.; Shibano, Y.; Tsuji, H.; Araki, Y.; Tamao, K.; Ito, O. Oligosilane Chain-Length Dependence of Electron Transfer of Zinc Porphyrin-Oligosilane-Fullerene Molecules. J. Phys. Chem. A 2007, 111 (16), 2973–2979. https://doi.org/10.1021/jp066749z.
20 Surampudi, S.; Yeh, M. L.; Siegler, M. A.; Hardigree, J. F. M.; Kasl, T. A.; Katz, H. E.; Klausen, R. S. Increased Carrier Mobility in End-Functionalized Oligosilanes. Chem. Sci. 2015, 6 (3), 1905–1909. https://doi.org/10.1039/c4sc03274h.
21 Kumagai, J.; Yoshida, H.; Ichikawa, T. Electronic Structure of Oligosilane and Polysilane Radical Cations as Studied by Electron Spin Resonance and Electronic Absorption Spectroscopy. J. Phys. Chem. 1995, 99 (20), 7965–7969. https://doi.org/10.1021/j100020a019.
22 Chernyavskii, A. I.; Buzin, M. I.; Chernyavskaya, N. A. Synthesis of Cyclolinear Permethylpolycarbosilanes with Oligosilane Fragments in the Backbone and Study of Their Properties. Russ. Chem. Bull. 2009, 58 (11), 2266–2270. https://doi.org/10.1007/s11172-009-0316-8.
23 A. Alec Talin, Andrea Centrone, Alexandra C. Ford, Michael E. Foster, Vitalie Stavila, Paul Haney, R. Adam Kinney, Veronika Szalai, Farid El Gabaly, Heayoung P. Yoon, François Léonard, and M. D. A. Tunable Electrical Conductivity in Metal-Organic Framework Thin-Film Devices.
24 Usov, P. M.; Jiang, H.; Chevreau, H.; Peterson, V. K.; Leong, C. F.; D'Alessandro, D. M. Guest-Host Complexes of TCNQ and TCNE with Cu3(1,3,5-Benzenetricarboxylate)2. J. Phys. Chem. C 2017, 121 (47), 26330–26339. https://doi.org/10.1021/acs.jpcc.7b07807.
25 Lüder, L.; Gubicza, A.; Stiefel, M.; Overbeck, J.; Beretta, D.; Sadeghpour, A.; Neels, A.; Nirmalraj, P. N.; Rossi, R. M.; Toncelli, C.; Calame, M. Conductive Hybrid Cu-HHTP-TCNQ Metal–Organic Frameworks for Chemiresistive Sensing. Adv. Electron. Mater. 2022, 8 (3), 2100871. https://doi.org/10.1002/aelm.202100871.
26 Traven, V. F.; Shapakin, S. Y. Charge-Transfer Complexes of Organosilicon Compounds. Adv. Organomet. Chem. 1992, 34 (C), 149–206. https://doi.org/10.1016/S0065-3055(08)60017-9.

27 Bande, A.; Michl, J. Conformational Dependence of σ-Electron Derealization in Linear Chains: Permethylated Oligosilanes. Chem. Eur. J. 2009, 15 (34), 8504–8517. https://doi.org/10.1002/chem.200901521.
28 Hong, D. H.; Suh, M. P. Enhancing CO 2 Separation Ability of a Metal-Organic Framework by Post-Synthetic Ligand Exchange with Flexible Aliphatic Carboxylates. Chem. - Eur. J. 2014, 20 (2), 426–434. https://doi.org/10.1002/chem.201303801.
29 Bueken, B.; Vermoortele, F.; Cliffe, M. J.; Wharmby, M. T.; Foucher, D.; Wieme, J.; Vanduyfhuys, L.; Martineau, C.; Stock, N.; Taulelle, F.; Van Speybroeck, V.; Goodwin, A. L.; De Vos, D. A Breathing Zirconium Metal-Organic Framework with Reversible Loss of Crystallinity by Correlated Nanodomain Formation. Chem. - Eur. J. 2016, 22 (10), 3264–3267. https://doi.org/10.1002/chem.201600330.
30 Reinsch, H.; Stassen, I.; Bueken, B.; Lieb, A.; Ameloot, R.; De Vos, D. First Examples of Aliphatic Zirconium MOFs and the Influence of Inorganic Anions on Their Crystal Structures. CrystEngComm 2015, 17 (2), 331–337. https://doi.org/10.1039/C4CE01457J.
31 Bueken, B.; Van Velthoven, N.; Krajnc, A.; Smolders, S.; Taulelle, F.; Mellot-Draznieks, C.; Mali, G.; Bennett, T. D.; De Vos, D. Tackling the Defect Conundrum in UiO-66: A Mixed-Linker Approach to Engineering Missing Linker Defects. Chem. Mater. 2017, 29 (24), 10478–10486. https://doi.org/10.1021/acs.chemmater.7b04128.
32 Bueken, B.; Vermoortele, F.; Vanpoucke, D. E. P.; Reinsch, H.; Tsou, C.-C.; Valvekens, P.; De Baerdemaeker, T.; Ameloot, R.; Kirschhock, C. E. A.; Van Speybroeck, V.; Mayer, J. M.; De Vos, D. A Flexible Photoactive Titanium Metal-Organic Framework Based on a [Ti IV 3 (μ 3 -O)(O) 2 (COO) 6] Cluster. Angew. Chem. Int. Ed. 2015, 54 (47), 13912–13917. https://doi.org/10.1002/anie.201505512.
33 Marshall, C. R.; Staudhammer, S. A.; Brozek, C. K. Size control over metal–organic framework porous nanocrystals *Chem. Sci.* 2019, 10, 9396–9408. https://doi.org/10.1039/C9SC03802G
34 Shearer, G. S.; Chavan, S.; Bordiga, S.; Svelle, S.; Olsbye, U.; Lillerud, K. P. Defect Engineering: Tuning the Porosity and Composition of the Metal−Organic Framework UiO-66 via Modulated Synthesis. Chem. Mater. 2016, 28 (11), 3749–3761. https://doi.org/10.1021/acs.chemmater.6b00602
35 Momeni, M. R.; Cramer, C. J. Structural Characterization of Pristine and Defective $[Zr_{12}(\mu_3\text{-}O)_8(\mu_3\text{-}OH)_8(\mu_2\text{-}OH)_6]^{18+}$ Double-Node Metal–Organic Framework and Predicted Applications for Single-Site Catalytic Hydrolysis of Sarin. Chem. Mater. 2018, 30, (13), 4432–4439. https://doi.org/10.1021/acs.chemmater.8b01913
36 Khoo, R. S. H.; Fiankor, C.; Yang, S.; Hu, W.; Yang, C.; Lu, J.; Morton, M. D.; Zhang, X.; Liu, Y.; Huang, J.; Zhang, J Postsynthetic Modification of the Nonanuclear Node in a Zirconium Metal–Organic Framework for Photocatalytic Oxidation of Hydrocarbons. J. Am. Chem. Soc. **2023** *145* (44), 24052–24060 https://doi.org/10.1021/jacs.3c07237
37 An, B.; Li, Z.; Song, Y.; Zhang, J.; Zeng, L.; Wang, C.; Lin, W. Cooperative copper centres in a metal–organic framework for selective conversion of CO_2 to ethanol. *Nat Catal 2019* **2**, 709–717. https://doi.org/10.1038/s41929-019-0308-5
38 Ji, P.; Manna, K.; Lin, Z.; Urban, A.; Greene, F. X.; Lan, G.; Lin, W. Single-Site Cobalt Catalysts at New $Zr_8(\mu_2\text{-}O)_8(\mu_2\text{-}OH)_4$ Metal-Organic Framework Nodes for Highly Active Hydrogenation of Alkenes, Imines, Carbonyls, and Heterocycles. J. Am. Chem. Soc., 2016, *138*, (37) 12234–12242. https://doi.org/10.1021/jacs.6b06759
39 Feng, D.; Jian. H.-L.; Chen, Y.-P.; Gu, Z.-Y.; Wei, Z.; Zhou, H.-C., Metal–Organic Frameworks Based on Previously Unknown Zr_8/Hf_8 Cubic Clusters. Inorg. Chem., 2013, 52 (21), 12661–12667. https://doi.org/10.1021/ic4018536
40 Peh, S.B.; Cheng, Y.; Zhang, J.; Wang, Y.; Chan, G. H.; Wang, J.; Zhao, D. Cluster nuclearity control and modulated hydrothermal synthesis of functionalized Zr_{12} metal–organic frameworks. Dalton Trans., 2019, 48, 7069–7073. https://doi.org/10.1039/C8DT05060K
41 Koschnick, C.; Stäglich, R.; Scholz, T.; Terban, M. W.; Mankowski, A. v.; Savasci, G.; Binder, F.; Schökel, A.; Etter, M.; Nuss, J.; Siegel, R.; Germann, L. S.; Ochsenfeld, C.; Binnebier, R. E.; Senker, J.; Lotsch, B. V. Understanding disorder and linker deficiency in porphyrinic zirconium-based metal–organic frameworks by resolving the Zr_8O_6 cluster conundrum in PCN-221. Nat. Commun., 2021, 12, 3099. https://doi.org/10.1038/s41467-021-23348-w
42 Bueken, B.; Van Velthoven, N.; Willhammar, T.; Stassin, T.; Stassen, I.; Keen, D. A.; Baron, G. V.; Denayer, J. F. M.; Ameloot, R.; Bals, S.; De Vos, D.; Bennett, T. D. Gel-Based Morphological Design of Zirconium Metal-Organic Frameworks. Chem. Sci. 2017, 8 (5), 3939–3948. https://doi.org/10.1039/c6sc05602d.

43 Xu, H.; Sommer, S.; Broge, N. L. N.; Gao, J.; Iversen, B. B. The Chemistry of Nucleation: In Situ Pair Distribution Function Analysis of Secondary Building Units During UiO-66 MOF Formation. Chem. - Eur. J. 2019, 25 (8), 2051–2058. https://doi.org/10.1002/chem.201805024.
44 Andreeva, A. B.; Le, K. N., Chen, L., Kellman, M. E., Hendon, C. H.; Brozek, C. K. Soft Mode Metal-Linker Dynamics in Carboxylate MOFs Evidenced by Variable-Temperature Infrared Spectroscopy. J. Am. Chem. Soc. 2020, 142 (45), 19291–19299. https://doi.org/10.1021/jacs.0c09499
45 Schneider, C.; Ukaj, D.; Koerver, R.; Talin, A. A.; Kieslich, G.; Pujari, S. P.; Zuilhof, H.; Janek, J.; Allendorf, M. D.; Fischer, R. A. High Electrical Conductivity and High Porosity in a Guest@MOF Material: Evidence of TCNQ Ordering within Cu_3BTC_2 Micropores. Chem. Sci. 2018, 9, 7405–7412. https://doi.org/10.1039/C8SC02471E.
46 Beltrán, J. I.; Flores, F.; Martínez, J. I.; Ortega, J. Energy Level Alignment in Organic–Organic Heterojunctions: The TTF/TCNQ Interface. J. Phys. Chem. C 2013, 117 (8), 3888–3894. https://doi.org/10.1021/jp306079t
47 Sini, G.; Sears, J. S.; Brédas, J.-L. Evaluating the Performance of DFT Functionals in Assessing the Interaction Energy and Ground-State Charge Transfer of Donor/Acceptor Complexes: Tetrathiafulvalene−Tetracyanoquinodimethane (TTF−TCNQ) as a Model Case *J. Chem. Theory Comput.* 2011, 7 (3) 602–609. https://doi.org/10.1021/ct1005517
48 Lin, S.; Usov, P. M.; Morris, A. J. The Role of Redox Hopping in Metal-Organic Framework Electrocatalysis. Chem. Commun. 2018, 54 (51), 6965–6974. https://doi.org/10.1039/c8cc01664j.
49 Marsmann, H.C.; Uhlig, F. in Chemical Shifts and Coupling Constants for Silicon-29, ed. Gupta, R.R; Lechner, M.D., Springer-Verlag, Berlin Heidelberg, 1st edn, 2008, Ch. 3, pp.1-34